



1 Geophysical fingerprint of the 4-11 July 2024 eruptive activity at 2 Stromboli volcano, Italy.

3
4 Luciano Zuccarello^{1,2}, Duccio Gheri¹, Silvio De Angelis^{2,1}, Riccardo Civico³, Tullio Ricci³, Piergiorgio
5 Scarlato³, Massimo Orazi⁴.

6 1Istituto Nazionale di Geofisica e Vulcanologia, Sezione di Pisa, via Cesare Battisti, 53, 56125, Pisa, Italy.

7 2School of Environmental Sciences, University of Liverpool, 4 Brownlow Street, L69 3GP, Liverpool, UK.

8 3Istituto Nazionale di Geofisica e Vulcanologia, Sezione di Roma1, via di Vigna Murata, 605, 00143, Roma, Italy.

9 4Istituto Nazionale di Geofisica e Vulcanologia, Osservatorio Vesuviano, via Diocleziano, 328, 80124, Napoli, Italy.

10 *Correspondence to:* Luciano Zuccarello (luciano.zuccarello@ingv.it); Duccio Gheri (duccio.gheri@ingv.it)

11 **Abstract.** Paroxysmal eruptions, characterized by sudden and vigorous explosive activity, are common events at many open-
12 vent volcanoes. Stromboli volcano, Italy, is well-known for its nearly continuous degassing activity and mild explosions from
13 the summit craters, occasionally punctuated by energetic, short-lived paroxysms. Here, we analyse multi-parameter
14 geophysical data recorded at Stromboli in early July 2024, during activity that led to a paroxysmal eruption on 11 July. We
15 use seismic, infrasound and ground deformation data, complemented by visual and Unoccupied Aircraft System observations,
16 to identify key geophysical precursors to the explosive activity and reconstruct the sequence of events. Elevated levels of
17 volcanic tremor and Very Long Period (VLP) seismicity accompanied moderate explosive activity, lava emission and small
18 collapses from the north crater, leading to a major explosion on 4 July, 2024 at 12:16 (UTC). Collapse activity from the North
19 crater area continued throughout July 7, while effusive activity occurred from two closely-spaced vents located on the Sciara
20 del Fuoco slope, on the Northwest flank of the volcano. On 11 July, a rapid increase in ground deformation preceded, by
21 approximately 10 minutes, a paroxysmal event at 12:08 (UTC); the explosion produced a 5 km-high eruptive column and
22 pyroclastic density currents along Sciara del Fuoco. We infer that the early activity in July was linked to eruption of resident
23 magma within the shallowest parts of the volcano plumbing. This was followed by lowering of the magma level within the
24 conduit system as indicated by the location of newly opened effusive vents. The rapid inflation observed before the paroxysmal
25 explosion on 11 July is consistent with the rapid expansion of gas-rich magma rising from depth, as frequently suggested at
26 Stromboli during energetic explosive events. Our results provide additional valuable insights into the eruptive dynamics of
27 Stromboli and other open-conduit volcanoes, and emphasize the importance of integrated geophysical observations for
28 understanding eruption dynamics, their forecasting and associated risk mitigation.

29 1 Introduction

30 Stromboli is an open conduit stratovolcano located in the Tyrrhenian Sea, off the northern coast of Sicily; its activity is
31 characterized by continuous degassing and frequent, small-to-moderate, explosions occurring every few minutes from the



32 summit craters, the well-known Strombolian activity. However, activity at Stromboli can rapidly escalate into more energetic
33 events, referred to as major explosions, which eject centimeter-to-meter-sized ballistic projectiles; at times, sustained explosive
34 activity is accompanied by partial collapses of the crater rim due to the instability of accumulated material, and increased
35 magmastatic pressure within the conduit system (Gurioli et al., 2013; Di Traglia et al., 2024). Since 2019, major explosions at
36 Stromboli have occurred with a frequency of about 4-5 events per year ejecting pyroclastic material to heights over a hundred
37 meters, which can travel beyond the summit crater area and potentially affect tourist paths (Rosi et al., 2013; Gurioli et al.,
38 2013). In heightened states of activity, Stromboli may also experience paroxysms, that is highly energetic eruptions that
39 generate eruptive columns exceeding 4 km in height, ballistics of up to 2 m in diameter and significant collapse activity from
40 the summit crater areas (Fig. 1). Paroxysms can be accompanied by the emplacement of pyroclastic density currents (PDCs)
41 along the Sciara del Fuoco (SdF, Fig. 1a), which can enter the sea and travel up to 2 km from the shoreline with demonstrated
42 potential to trigger tsunamis (Rosi et al., 2006; Calvari et al., 2006; D'Auria et al., 2006; Ripepe and Lacanna, 2024). Although
43 paroxysms are less frequent than major explosions, with an average occurrence of just one every four years since 2003, they
44 are the most impactful hazard for the island of Stromboli (Rosi et al., 2013). A recent paroxysm on 3 July, 2019, resulted in a
45 fatality (Giudicepietro et al., 2020; Giordano and De Astis, 2020; Andronico et al., 2021).

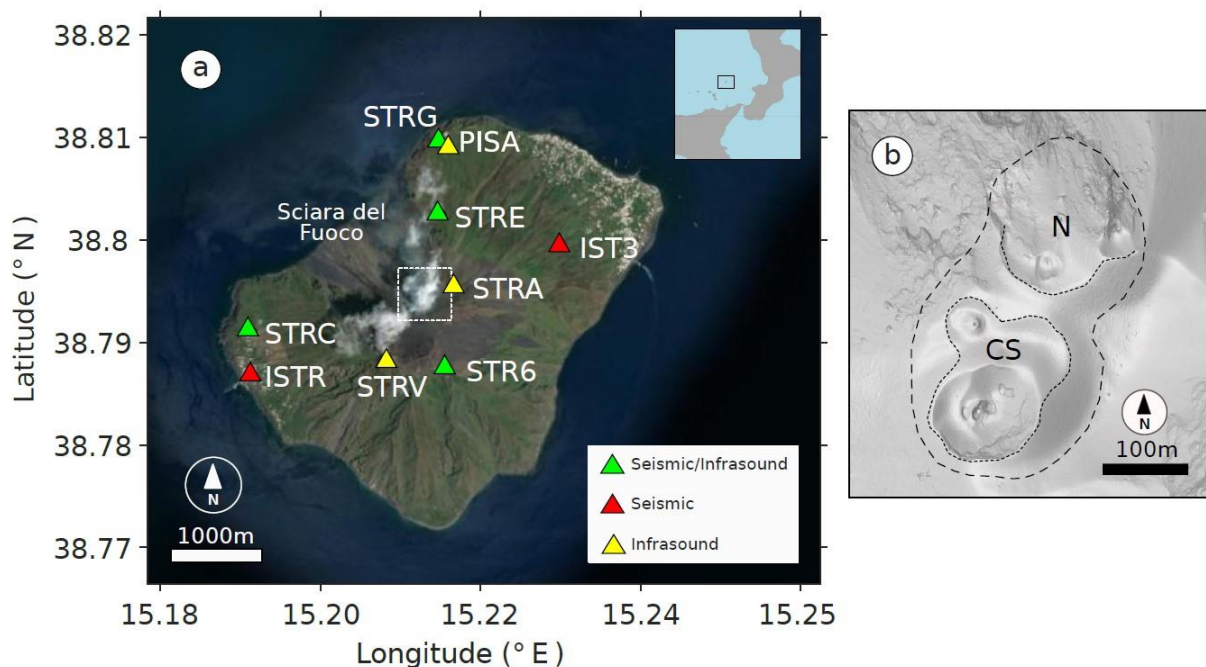
46 Unrest and eruption at Stromboli generate a broad range of geophysical signals. Nucleation and coalescence of gas bubbles
47 into gas slugs (Sparks, 2003; Burton et al., 2007; Caricchi et al., 2024), and their ascent within the conduit generates
48 characteristic seismic and deformation signals (Marchetti et al., 2009); gas slug bursting at the top of the magma column
49 produces infrasound waves (Colò et al., 2010). Real-time detection and monitoring of these signals are crucial for risk
50 mitigation at Stromboli as, in the recent past, major explosions and paroxysms have frequently been anticipated by detectable
51 changes in geophysical signals between tens of seconds and minutes before their occurrence (Giudicepietro et al., 2020; Ripepe
52 et al., 2021a; Longo et al., 2024).

53 Except for the 2019 eruptive activity, the most intense in recent years, Stromboli's paroxysms are typically preceded by periods
54 of lava effusion, or a general increase in surface activity that lasts for several days (Ripepe et al., 2009; Valade et al., 2016).
55 Several studies have suggested that effusive eruptions may act as a trigger for paroxysmal explosions through a mechanism of
56 decompression of the volcano plumbing system, evidenced by a drop in magma levels within the conduit (Aiuppa et al., 2010;
57 Calvari et al., 2011; Ripepe et al., 2017). The most significant effusive event in terms of its volume occurred between December
58 2002 and July 2003 (Ripepe et al., 2017), which caused landslides, triggered a partial collapse of the SdF and culminated in a
59 paroxysm on 5 April, 2003; this was the first large-scale paroxysmal event on record since 1985 (Calvari and Nunnari, 2023).
60 However, it should also be noted that effusive eruptions are not necessarily followed by paroxysms. An example is the
61 November 2014 effusive eruption, which did not lead to paroxysmal activity (Rizzo et al., 2015). At the other end of the
62 spectrum lies the paroxysm of July 2019, for which no clear increase in activity prior to the main event was recorded. As
63 highlighted by Laiolo et al. (2022), thermal and gas flow levels had slightly increased but remained below "alert" thresholds.
64 Multi-parameter data are crucial to understand unrest at Stromboli and to detect transitions between low-to-moderate activity
65 and more explosive phases (Pistolesi et al., 2011; Andronico et al., 2021). Several conceptual models have been proposed



66 accounting for the ordinary seismic activity observed at Stromboli and other similar volcanoes (e.g., Chouet et al., 2008;
67 Suckale et al., 2016; Ripepe et al., 2021b). Petrological analyses of erupted products suggest the presence of a stratified conduit
68 at Stromboli, consisting of two types of magma (Bertagnini et al., 2003; Francalanci et al., 2004; Francalanci et al., 2005). The
69 upper conduit is thought to host highly porphyritic (HP) magma that is water-poor and rich in phenocrysts, and is erupted as
70 scoria during ordinary activity; on the other hand, magma in the lower conduit is gas-rich, low-porphyritic (LP), and typically
71 erupted as pumice alongside HP scoria and lithic blocks removed from conduit walls. Eruptive activity at Stromboli is inferred
72 to be controlled by the buoyant ascent and bursting of gas slugs (Sparks, 2003; Burton et al., 2007; Caricchi et al., 2024;
73 Aiuppa et al., 2010) from the top of the LP magma, rising through the more crystalline HP magma acting like a viscous fluid
74 or a rigid plug and controlling the final ascent and explosion of the slugs (Suckale et al., 2016). A recent model by (Caricchi
75 et al., 2024) shows that the instability of gas-rich and low-density foam layers at the base of the magma column could also
76 potentially trigger paroxysmal explosions at open conduit volcanoes.

77 In this study, we report on the most recent paroxysm at Stromboli, which occurred on 11 July, 2024, after a month of unrest at
78 the summit craters, as reported by the Istituto Nazionale di Geofisica e Vulcanologia (INGV) (INGV-OE, 2024). We analyze
79 the precursory geophysical activity leading up to the paroxysm based on seismic, infrasound and ground deformation data
80 gathered by the INGV monitoring network, complemented by observations conducted with an Unoccupied Aircraft System
81 (UAS) during the study period. The UAS imagery provides a valuable tool to interpret geophysical data and understand the
82 conditions leading up to the paroxysm on 11 July, offering a high-resolution reconstruction of the eruptive events and
83 associated morphological changes at the volcano. Unless, otherwise stated, all descriptions of surface activity in this
84 manuscript are from direct field observations by the authors during the study period.



85



86 **Figure 1: a) Map of monitoring network at Stromboli, showing the locations of seismo-acoustic, seismic, and infrasound sensors.**
87 **The inset shows the location of Stromboli volcano in Italy (MATLAB-Mapping Toolbox). b) Detail of the summit area of Stromboli,**
88 **corresponding to the white dash-line square in a), showing the summit crater areas.**

89 **2 Chronology of eruptive activity during 3-11, July, 2024**

90 The activity bulletins issued by INGV (see Data Availability), from May 24 until the early days of July, reported an increase
91 in surface activity at Stromboli, particularly from the North (N) crater area (Fig. 1b), characterized by continuous and intense
92 spattering, that is quasi-continuous emission of pyroclastic material through sequential, small-to-moderate, explosions ejecting
93 ballistics at heights of ~10-20 m above the vent (Harris and Ripepe, 2007; Giudicedipietro et al., 2021) (Fig. 2a). The average
94 frequency of explosions fluctuated between 13 (medium) and 16 (high) events/hour with spattering occasionally leading to
95 lava flows along the SdF (Fig. 1a). On June 23 and 28, lava flows began, following intense spattering from the N crater,
96 converging into a canyon-like structure created by previous PDC activity in October 2022 (Di Traglia et al., 2024). Sulfur
97 dioxide (SO₂) and carbon dioxide (CO₂) emissions remained at average levels, as did the carbon-to-sulfur (C/S) ratio (INGV-
98 OE, 2024).

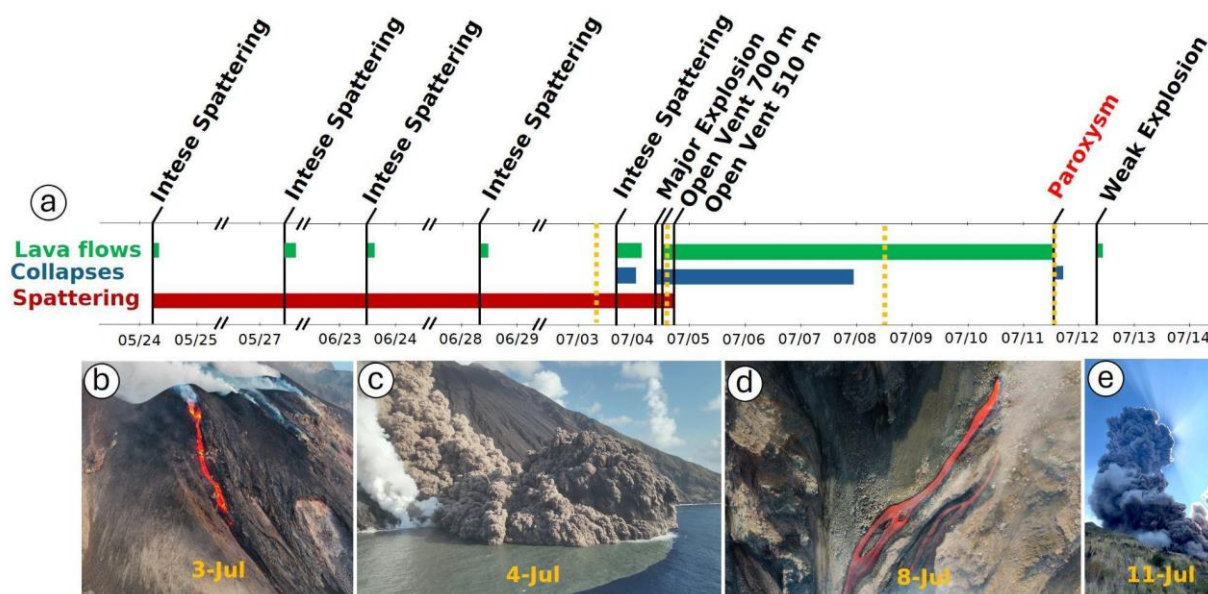
99 On 3 July, at 16:35 UTC, intense spattering was observed from a vent located within the N crater sector, leading to a sequence
100 of partial collapses of the N crater rim, which also remobilized material that had been erupted in the preceding days. These
101 collapses mostly consisted of cold material with a minor contribution of hot deposits. At 17:02 UTC, a lava flow began from
102 the same vent, accompanied by spattering and moderate explosions (Fig. 2b). The activity continued throughout the night, with
103 lava fronts moving down to an elevation of 550-600 m a.s.l..

104 On 4 July, at 12:16 UTC, a major explosion occurred from the N crater and, at 14:10 UTC, a new lava flow emerged at the
105 base of the N crater area at ~700 m a.s.l., advancing towards Bastimento and Filo di Fuoco, located along the northeast
106 boundary of SdF. After about one hour a second lava flow started at an elevation of ~580 m a.s.l., which reached the sea. At
107 16:15 UTC, another vent opened at ~510 m a.s.l., producing a third lava flow accompanied by PDCs that rapidly descended
108 the SdF into the sea (Fig. 2c). During the evening of 4 July, and throughout the following night, lava flow activity continued,
109 accompanied by occasional collapses of pyroclastic materials.

110 Between 5-6 July, 83 landslide events were observed, while effusive activity fluctuated and lava emission moved further
111 downslope originating from two new eruptive vents at ~485 m a.s.l. (Fig. 2d). The flow formed a delta at the shoreline and
112 steam plumes were observed caused by magma-seawater interaction. Explosive activity from the summit craters halted at the
113 beginning of the effusive phase.

114 On 11 July, at 12:08 UTC, a paroxysmal eruption occurred from the N crater area, producing an ash plume mn ~5 km high,
115 which dispersed towards the southwest (Fig. 2e). Shortly after, a pyroclastic flow rapidly advanced along the SdF, which
116 triggered a small-scale tsunami wave. The paroxysmal phase ended with a series of secondary and less intense PDCs.

117 In the following hours, effusive activity ceased, and no further explosions were observed, except for a minor event on 12 July,
118 at 08:28 UTC (Fig. 2a), which was followed by a small collapse event in the N crater area.



119

120 **Figure 2: Timeline of the observed surface activity and key visual observations at Stromboli between late May and mid-July, 2024.**
121 **a)** Timeline showing the chronology of activity, which marks periods of activity characterized by lava flows (green), collapses (blue)
122 and spattering (red). Significant events are labelled, such as intense spattering, a major explosion on 4, July, opening of new vents,
123 and the paroxysm on 11, July. **b-e)** Sequence of images gathered at the times indicated by the dashed yellow lines in **a)**. From left to
124 right: spattering activity on 3, July, a PDC event reaching into the sea on 4, July, continued lava flow on 8, July, and the paroxysmal
125 explosion on 11, July (photo “e” courtesy of G. De Rosa - OGS).

126 3 Geophysical observations

127 In this study we use data recorded by the geophysical monitoring network deployed and maintained on Stromboli by INGV
128 (Fig. 2a). The network includes seismic (ISTR3, ISTR) and infrasound sensors (STRA, STRV), as well as seismo-acoustic
129 stations (STR6, STRC, STRE, STRG). An additional infrasound sensor, PISA (Gheri et al., 2024), was deployed on 4 July at
130 13:35 UTC, 35 minutes before the onset of the effusive activity.

131 3.1 Seismic characterization of unrest and eruptive events

132 Volcanic tremor is traditionally thought to reflect magma movement within the conduit (McNutt and Nishimura, 2008; Chouet
133 et al., 1997; Ripepe and Gordeev, 1999); at Stromboli, tremor is routinely monitored by means of the Root Mean Square (RMS)
134 of the continuous seismic signal in the 1-3 Hz frequency band (Giudicepietro et al., 2023). Figure 3a shows RMS values of the
135 order of 10^{-6} ms⁻¹ (recorded at the IST3 site), which correspond to tremor classified by INGV as high. A marked and short-
136 lived increase in seismic RMS was observed after the major explosion at 12:11 on 4 July (Fig. 3a). During this period, the
137 signal reached unprecedented levels, peaking at 10^{-4} m s⁻¹ at 17:00 UTC. Short-lived increases in RMS values were still noted

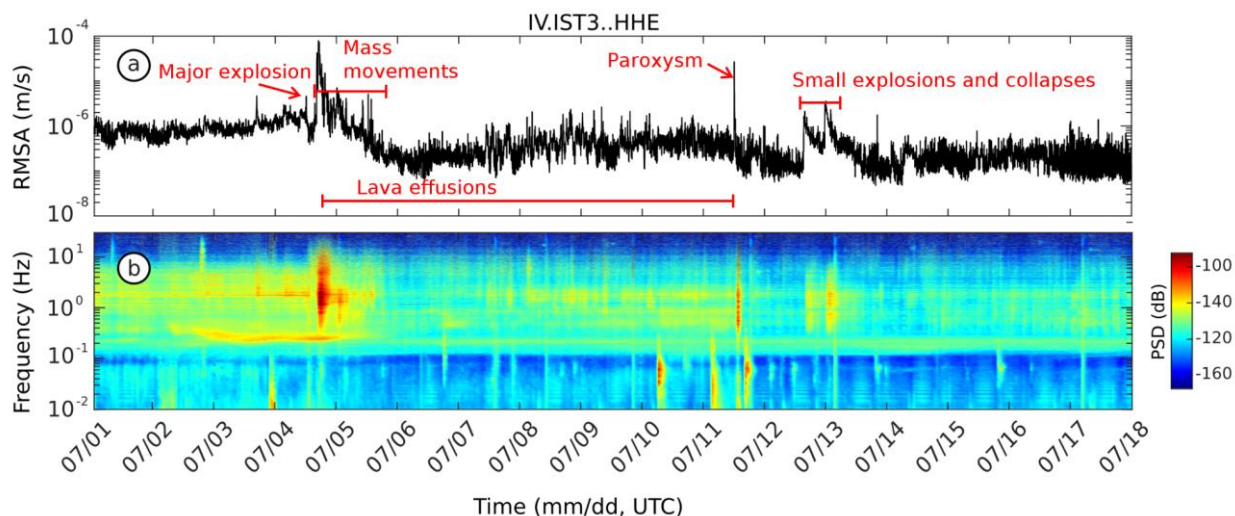


138 throughout 5, July, although the amplitudes exhibited an overall decline to values of the order of 10^{-7} m s⁻¹, lower than those
139 recorded at the beginning of July. In the following days (6-11, July), the tremor was marked by a series of short-duration peaks
140 during lava flow activity. This behavior changed again on 11, July, when the onset of paroxysmal activity coincided with a
141 new increase in RMS (Fig. 3a). After the paroxysm, the RMS decreased again with only sparse and brief intervals of increased
142 amplitudes between 12-13, July (Fig. 3a). From late on 13 July, onwards, the amplitude stabilized around 10^{-7} m s⁻¹, indicating
143 that volcanic activity had reduced and returned to background levels. Additional details of the signals recorded on 4-7 July,
144 are shown in the Supplementary Materials (Fig. 1S).

145 The spectrogram in Fig. 3b shows nearly continuous energy in the 2-3 Hz range, typically associated with tremor signals at
146 Stromboli (Ripepe et al., 1996). Energy levels in this band change throughout the pre-, syn-, and post-explosive activity
147 periods, reaching a maximum on 4 July following the major explosion. A pulsating phase was observed from 6-11 July, with
148 another peak during the paroxysm. Explosive activity between 4-11, July, exhibited a broader frequency range in the 0.5-15
149 Hz band. It is worth noting that the eruptive event on 4, July was preceded by a high-energy signal in the narrow frequency
150 band 0.2-0.3 Hz (Fig. 3b). We also observe that this very low-frequency signal was not recorded before the paroxysm on 11,
151 July. Finally, on July 10 at 05:09 UTC and on 11 July at 02:26 and 15:21 UTC, high-energy signals were observed around
152 0.05-0.08 Hz, exhibiting a dispersive spectrum typical of teleseismic events as reported by USGS (for further information, see:
153 <https://earthquake.usgs.gov/earthquakes/search/>).

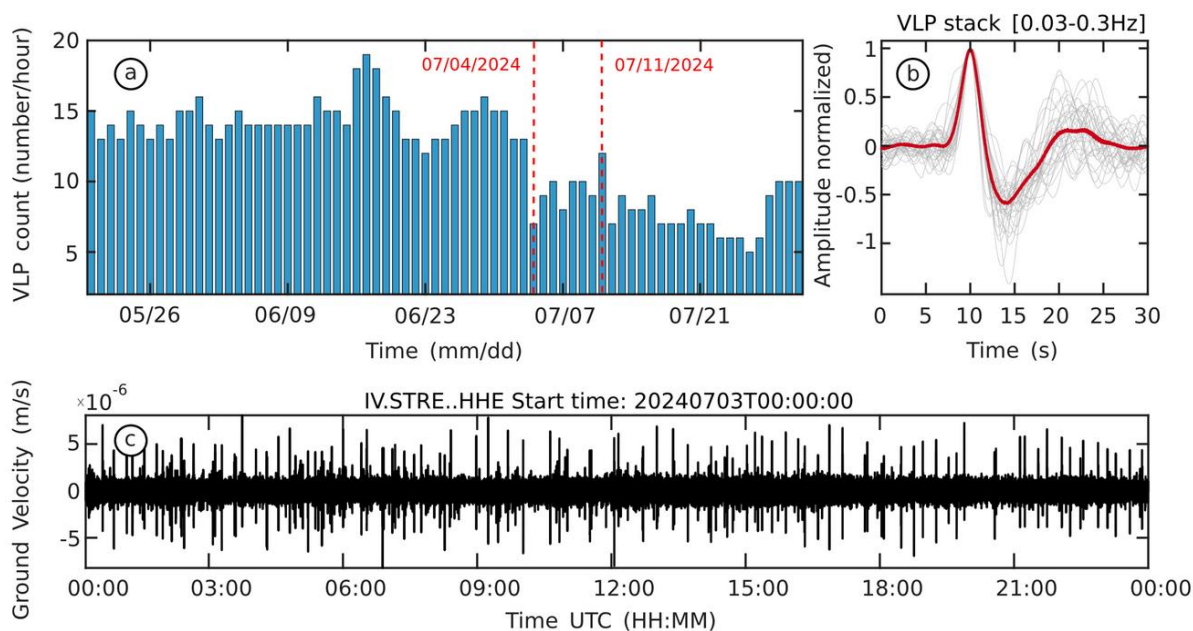
154 We have also analysed the occurrence of Very Long Period (VLP) earthquakes that have traditionally been associated with
155 pressure disturbances and the dynamics of gas-rich magma within fluid-filled structures (Chouet et al., 1997; Chouet et al.,
156 1999; Marchetti and Ripepe, 2005; Legrand and Perton, 2022), and one of the main tools used to monitor unrest at Stromboli.
157 An increase in the frequency of occurrence of these signals is typically a precursor to periods of elevated eruptive activity
158 (Ripepe et al 2009; Delle Donne et al., 2017). Figure 4a derived from information sourced from the INGV bulletins (INGV-
159 OE, 2024), provides an overview of the rates of VLP seismicity at Stromboli between the end of May and mid-July 2024, after
160 the 11 July paroxysm. From May until mid-June, VLP event rates remained stable, fluctuating around high values between 12
161 and 19 events/hour. A mean rate of ~ 13 events/hour is defined, at Stromboli, as “normal activity” (Ripepe et al., 2008) and it
162 suggests that an efficient degassing mechanism of the magma column is established (Ripepe et al., 2021b). A significant peak
163 is observed around mid-June, with the number of VLP events reaching a high of 19 events/hour on June 16. This peak is
164 followed by a slight decrease in event rates, although the number of events remained elevated compared to previous days.
165 Figure 4b shows the characteristic compression-decompression cycle of VLP events at Stromboli; this waveform represents
166 the normalized stack of all VLP events with maximum amplitude greater than 5×10^{-6} m s⁻¹ at station STRE. Figure 4c shows
167 a 1-day filtered (0.03-3Hz) seismic record illustrating the occurrence of VLP events as recorded at station STRE, on the east
168 flank of SdF at 495 m of elevation (see Fig. 1).

169 Before the major explosion on 4 July, we observed a clear drop in the occurrence of VLP events (Fig. 4a) from 10-15 to 7-10
170 events/hour. The rates of VLP events remained stable until the 11 July paroxysm, peaking again at 12 events/hour on that day.
171 After the paroxysm, a further decrease in VLP rates was observed with hourly counts ranging from 6 to 10 events.



172

173 **Figure 3:** a) Seismic tremor or RMS calculated every minute using a moving time window of 5 minutes, within the volcanic tremor
 174 frequency band of Stromboli (1-3 Hz), from July 2 to 18. b) Spectrogram of the E-component from the IST3 seismic station for the
 175 same period.



176

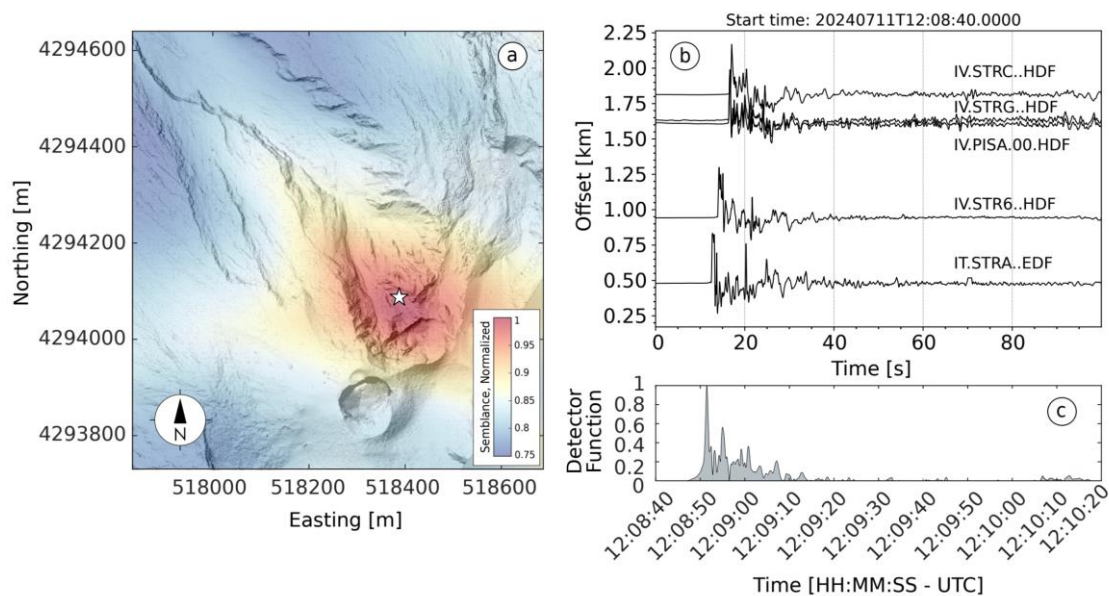
177 **Figure 4:** a) Hourly rates of VLP events from the INGV catalog. Vertical red dashed lines indicate the major explosion and paroxysm
 178 that occurred on 4 and 11, July, respectively. b) VLP waveform events ($>5 \times 10^{-6}$ m s $^{-1}$) recorded on 3, July, at station STRE
 179 normalized with respect to maximum amplitude (light grey). The red waveform represents the average of all high-amplitude
 180 waveforms. c) Continuous waveform recorded at station STRE (EW component) on 3, July 2024, filtered between 0.03-0.3 Hz.



181 3.2 Infrasound characterization of unrest and eruptive events

182 We have also analysed infrasound data recorded by the INGV acoustic monitoring network and an additional microphone
183 installed during the period of activity (Fig. 1). The infrasonic record before 4, July, shows a typical background of moderate
184 strombolian activity occasionally interspersed with larger explosions (see Fig. 2Sa). The major explosion on 4 July, generated
185 an infrasonic transient with a pressure of 5 Pa (Fig. 2Sb) at station STR6, from the CS crater area. Following this event, a
186 marked decrease in acoustic energy was observed until the 11, July paroxysmal event, which produced infrasonic waves with
187 a peak amplitude of 115 Pa at the STR6 site (approximately at ~750 m, see Fig.1a and Fig.2Sb).

188 We have used the infrasound records from all operating sensors of the INGV monitoring network on Stromboli and an
189 additional temporary microphone (Fig. 2) to locate the source of the paroxysmal eruption on 11, July 2024. We employed the
190 RTM-FDTD (Reverse Time Migration - Finite Difference Time Domain) method of Fee et al. (2021), which implements
191 waveform back-projection over a grid of candidate source locations. Travel-times between potential source locations and all
192 stations in the network are calculated via FDTD modeling (Kim and Lees, 2014; Fee et al., 2017; Diaz-Moreno et al., 2019)
193 to account for the effect of topography on the propagation of the acoustic wavefield. In the RTM-FDTD method, waveforms
194 are back-projected and a detector function (e.g., network stack, network semblance) is evaluated for each candidate source,
195 with the detector maximum corresponding to the most likely location. For FDTD calculations of travel-times we employed a
196 UAS-derived Digital Elevation Model (DEM) of the SdF and the summit craters (Civico et al., 2024) areas conducted on the
197 morning of 4 July with initial individual resolutions ranging between 20 and 50 cm/pixel. This DEM was merged with a
198 basemap elevation model (Civico et al., 2021) of the rest of the island, re-sampled, and parsed into a 5x5 m grid for the purpose
199 of FDTD modeling. For FDTD modeling, the source time function was approximated by a Blackman-Harris function with a
200 cutoff frequency of 5 Hz (high enough to include the dominant frequency of the explosion signals while still allowing time-
201 efficient computing) and the acoustic wavefield was propagated along the discretized topography using 15 grid points per
202 wavelength (Wang, 1996). We used a constant sound velocity of 330 m s⁻¹ (estimated from the signal move-out across the
203 network) and a stratified atmosphere model based on density and temperature data obtained from the Reanalysis v5 (ERA5)
204 dataset (see Data and Resources), produced by the European Centre for Medium-Range Weather Forecasts of the Copernicus
205 Climate Change Service. We used data corresponding to the ERA5 grid node closest to Stromboli, at 12:00 on 11, July 2024
206 (Coordinated Universal Time, UTC). The inferred source location for the paroxysmal explosion on 11, July 2024, along with
207 a record section of the infrasound waveforms used and the detector function, are shown in Fig. 5. The location identifies a
208 source located approximately 50m below the rim of the N crater (Fig. 5a) at an elevation of ~685 m. The estimated origin time
209 for the event is 12:08:52 UTC.



210

211 **Figure 5: Infrasound location of the 11 July, 2024 paroxysmal event using the RTM-FDTD method (see manuscript for details; DEM**
212 **of July 14, 2024 from Civico et al. (2024). a) Map-view of network semblance maximum around the Stromboli crater region. RTM-**
213 **FDTD semblance location is indicated by a white star; b) record section of the filtered infrasound waveforms (bandpass filter 0.01-**
214 **15Hz) used for locating the event. The offset corresponds to source-station distance; c) Normalized network detector function (i.e.,**
215 **maximum network semblance amplitude over time).**

216 3.3 Deformation of unrest and eruptive events

217 Ground tilt at Stromboli has been frequently inferred to reflect processes like slug coalescence, slug ascent, and conduit
218 emptying (Marchetti et al., 2009; Genco and Ripepe, 2010; Bonaccorso, 1998). Over the last decade, tilt has become central
219 to real-time monitoring and eruption early warning at Stromboli. Ripepe et al. (2021a), for example, demonstrated the scale
220 invariance of tilt at Stromboli, that is all explosions, regardless of their intensity, follow the same ground inflation-deflation
221 pattern. A significant tilt was reported on 4 July (INGV-OE, 2024). The major explosion at 12:00 UTC was accompanied by
222 a characteristic inflation-deflation pattern (Longo et al., 2024), followed by a pronounced deflation trend that began at 16:20
223 UTC and continued until 19:50 UTC (INGV-OE, 2024).

224

225 For the paroxysm on 11, July 2024 fig. 5 shows the seismic-derived tilt, reconstructed from the EW horizontal component
226 record at station STRE Aoyama et al. (2008), Genco and Ripepe (2010), and De Angelis and Bodin (2012). Slow inflation is
227 observed, starting approximately 600 seconds before the explosion (Fig. 5b); the seismic-derived tilt sharply accelerates
228 approximately 1 minute before reaching its peak of 1.5 μ rad at the onset of the explosion, followed by rapid deflation. This
229 pattern is consistent with previous observations of tilt at Stromboli before paroxysms and major explosions (e.g. Genco and
230 Ripepe (2010); Ripepe et al. (2021a)). We note that this tilt signal is derived from an individual seismic record, of an instrument



231 that is not likely oriented in the direction radial to the source; for this reason, we will focus on the interpretation of the
232 deformation trend, and will not use the measured tilt amplitude for modelling purposes.

233 **4 Discussion**

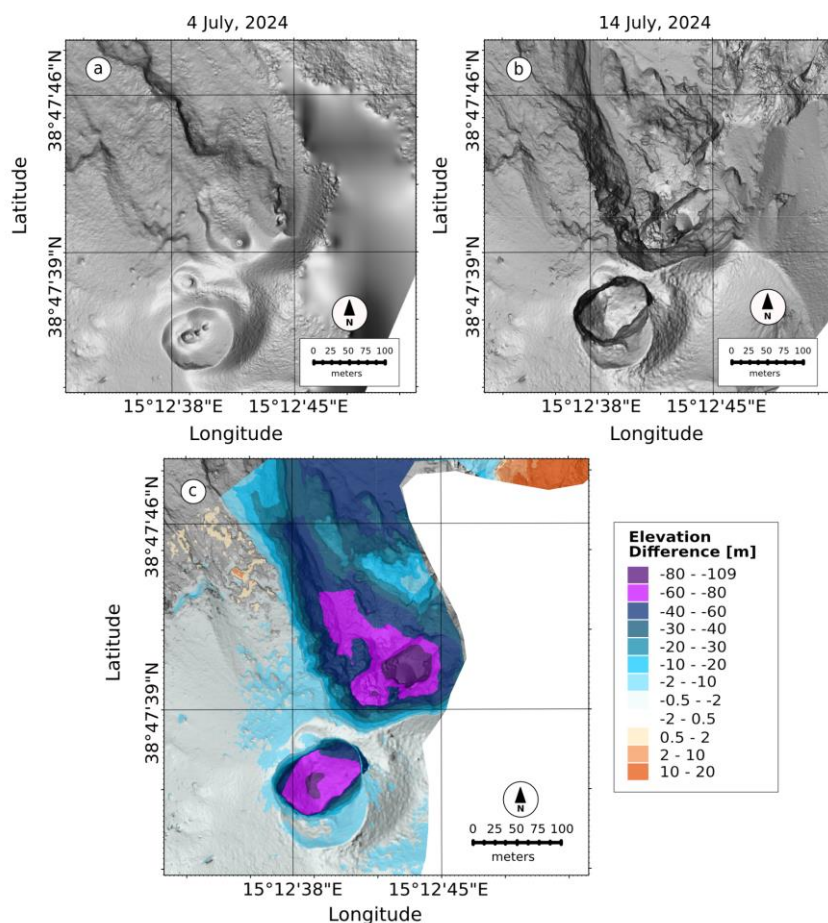
234 In this manuscript we have presented geophysical data recorded between early and mid-July 2024 at Stromboli; the period of
235 unrest included a major explosion on 4 July, significant collapse activity in the N summit crater area, emplacement of lava
236 flows, and a paroxysmal event on 11 July. Surface activity at Stromboli intensified late in May with a marked increase in the
237 occurrence of Strombolian explosions, the onset of effusive activity from SdF, and increasing volcanic tremor. Early in July,
238 we observed a steady increase in volcanic tremor reaching unprecedented amplitudes on 4 July, (see Fig. 3a and Fig. 1S).
239 Volcanic tremor at Stromboli has typically been linked to the coalescence of gas bubbles from layers of smaller bubbles and
240 their ascent along the shallower conduit (McNutt et al., 2008; Chouet et al., 1997; Ripepe et al., 1999), suggesting that
241 variations in tremor intensity are controlled by changes in gas flow within the conduit. It has been frequently speculated that
242 an increase in volcanic tremor reflects an increase in the volume of gas within the magma (Ripepe et al., 1996), which in turn
243 is linked to a higher occurrence of explosions at the top of the magma column. Field observations of increasing spattering in
244 early July (Fig. 1) support a model of increased surface activity linked to the ascent of gas-rich magma within the shallow
245 conduit. The high rates of VLP events observed during the same period further support the hypothesis of gas-rich magma
246 migration within the shallow plumbing system. These events are traditionally associated with the rapid expansion of gas slugs
247 rising through the liquid melt in the shallow conduit (Chouet et al., 2003; James et al., 2006); more recently (Ripepe et al.,
248 2021) suggested that VLP waveforms at Stromboli are generated at the top of the magma column, mainly after the onset of
249 Strombolian explosions; they showed that the occurrence of VLP event can be linked to explosive magma decompression in
250 the uppermost ~ 250 m of the conduit. The recorded VLP events showed similar waveforms (Fig. 4b) suggesting a stable source
251 mechanism and location; locations in the shallow parts of the conduit can be linked to magma accumulation at a shallow depth,
252 close to the surface. While the number of VLP events did not show any significant variation before the major explosion on 4
253 July, volcanic tremor increased slowly but steadily (Fig. 3a). Coinciding with strong ground deflation after the major explosion
254 (INGV-OE, 2024), volcanic tremor reached an unprecedented peak amplitude of $\sim 8 \times 10^{-5}$ m s⁻¹ at ~17:00 UTC associated
255 with the opening of a new effusive vent at ~ 510 m elevation within SdF (Fig. 2a) and the occurrence of numerous mass
256 wasting events linked to collapse activity within the lower N crater area and upper section of SdF. We suggest that these signals
257 reflect the emptying of the shallowest parts of the conduit system and the overall lowering of the magma level within the
258 shallow volcano plumbing reflected in the opening of new effusive vents at progressively lower elevations. The transition
259 between explosive and effusive regimes was also marked by a clear decrease in the occurrence of VLP events (Fig. 4), and a
260 migration of their source deeper within the conduit (Ripepe et al., 2015). This contrasts with the flank eruptions of 2007 and
261 2014 (Ripepe et al., 2009; Ripepe et al., 2015) when VLP rates remained high during effusion; in July 2024 it appears that
262 effusion reduced the overall explosivity, rather than recalling fresh magma from depth. The new effusive regime, indeed, was



263 characterized by a substantial lack of Strombolian explosive activity at the surface between 4-11 July, as observed in the field
264 by our research team. The quasi-continuous collapse activity, observed from 13:00 UTC on 4, July, appeared to be linked to
265 instabilities in the crater area around newly created vents; this instability persisted in the following days, with the number of
266 events peaking on July 5 (83 recorded occurrences recorded in a single day (INGV-OE, 2024). The collapse activity recorded
267 along the N crater rim, adjacent to the SdF, resulted in significant changes to the morphology of this sector of the volcanic
268 edifice (Fig. 6).

269 During the study period, we also collected UAS data and compiled very high-resolution repeat DEMs (0.2-0.5 m/pixel), which
270 allowed quantifying topographical changes via DEM differencing. The difference between DEMs on 4, July, (morning) and
271 July 14 is shown in Fig. 7c. The data processing methodology follows the procedures described in Civico et al. (2022, 2024).
272 The most notable morphological variations were observed in the afternoon of 4 July, while the paroxysm on 11 July did not
273 lead to significant changes.

274 The summit craters were affected by loss of material due to the opening of two eruptive vents at approximately 700 and 500
275 m a.s.l.. While the CS crater sector showed a roughly circular-shape crater floor deepening of about 84 m, the N sector was
276 affected by the complete dismantling of its northern rim and external slope, marking the deepest morphological change
277 occurred at the summit craters in the last decades, with a maximum difference in altitude of 109 m. The total volume loss
278 recorded in the summit craters sector was estimated at 3.3 Mm³ (Civico et al., 2024).



279

280 **Figure 6: Multidirectional hillshades of Stromboli's crater area: a) 4, July 2024 (Civico et al., 2024c), b) July 14, 2024 (Civico et al.,**
281 **2024), c) map of elevation difference (Dem of Differences) highlighting morphological changes occurred between 4 and 14 July, 2024.**
282 **Purple areas indicate material loss, whereas orange areas indicate material gain.**

283 Unlike the summit craters, the subaerial portion of the SdF slope was affected by both accumulation and erosion processes.
284 Here, the main loss of material (2.74 Mm³; Civico et al., 2024a) was localized along the canyon formed in October 2022 (Di
285 Traglia et al., 2024), which has widened and deepened during the July 2024 eruption. Accumulation processes instead were
286 mainly due to PDC and lava flow deposits, localized in the northeastern sector of the slope. The maximum accumulation of
287 lavas occurred at the new lava delta (maximum difference in altitude of 45 m), located in the center of the SdF shoreline.
288 The effusive regime ended with the occurrence of the paroxysmal explosion on 11, July. The explosion generated an infrasonic
289 pressure of 115 Pa at station STR6 with an associated VLP amplitude reaching $5.8 \times 10^{-5} \text{ m s}^{-1}$ (see Fig. 3S). An ash plume
290 reached a height of 5 km above the vent, and pyroclastic flows moved down the SdF. After that, volcanic activity reduced its
291 intensity, showing low levels of tremor and VLP events although the tremor increased again on 12, July, associated with a
292 small lava flow.



293 The eruptive crisis of July 2024, culminating in the paroxysm, is consistent with previous eruptions at Stromboli, such as those
294 in April 2003, March 2007, and July-August 2019. The data discussed above can be used to inform a conceptual model of the
295 entire sequence of processes responsible for the observed surface and eruptive activity, within the framework of previous
296 studies (e.g., James et al., 2006; Chouet et al., 2008; Del Bello et al., 2012; Suckale et al., 2015; McKee et al., 2022).

297 The spattering activity, observed at the start of our study period, represents an intensified form of puffing. Spattering activity
298 results from the quasi-continuous bursting of small gas pockets within a bubbly flow regime, which generates pyroclasts
299 fragments (Rosi et al., 2013). This activity typically marks the initial stages of unrest and eruption at Stromboli, where gas-
300 rich magma is being actively degassed through continuous explosive bursts (Del Bello et al., 2012). At the more explosive end
301 of the spectrum of Strombolian activity major explosions and paroxysms are often explained invoking the "slug model" (James
302 et al., 2006; Chouet et al., 2008; Del Bello et al., 2012). In this model, gas bubbles (slugs) form deeper in the magma column
303 and gradually coalesce as they rise through the conduit due to an increase of the magma viscosity. As gas slugs ascend, they
304 expand due to decreasing pressure and eventually reach the surface. When they burst at the top of the magma column, they
305 release gas explosively, fragmenting the magma and producing pyroclasts and feeding ash plumes of varying sizes. After the
306 major explosion on 4 July, an effusive regime was established, characterized by lava flows, during which more degassed
307 magma was erupted. Following the initial explosive activity driven by gas slugs, we infer that the transition to effusive regime
308 is controlled by depressurization of the shallow plumbing system similar to Ripepe et al. (2017). The depressurization of the
309 system caused by the initial explosive activity allowed magma to flow, and reach the surface forming lava flows, without
310 further explosive activity. As the shallow volcanic conduit progressively emptied it leads to structural instability, causing
311 collapses and landslides along the SdF.

312 According to Ripepe et al. (2017), the emptying of the conduit creates a vacuum effect that draws more gas-rich magma from
313 deeper within the system. As volatile-rich magma rises and encounters lower pressures, it can lead to explosive eruptions,
314 resulting in a paroxysmal event. The dynamics of the 11, July paroxysmal explosion displayed similar trends across seismic,
315 acoustic, and deformation parameters compared to the others (Genco and Ripepe, 2010; Ripepe et al., 2021a). This consistency
316 further validates the established models of Strombolian activity, where the largest explosions and energetic events, such as
317 paroxysms, are driven by the same source mechanism. The scale-invariant conduit dynamics of ground deformation
318 demonstrate that inflation amplitude and duration scale directly with the magnitude of the explosion (Ripepe et al., 2021a).
319 Ground deformation observed on 11, July (Fig. 5) follows the same exponential inflation pattern as seen in previous paroxysms
320 (Ripepe et al., 2021a). This behavior is typically explained by bubble dynamics, where the pressure on the conduit walls
321 increases due to the rapid volumetric expansion of gas in highly vesiculated magma. As gas rises and expands, moreover, it
322 pushes the magma column toward the surface, often leading to precursory lava emissions from the vent. Ground deformation
323 is likely caused by a combination of increasing magma static pressure and the pressurization of degassed magma at the top of
324 the column, driven by the exponential growth of gas. When the pressure applied by the gas-rich magma exceeds the tensile
325 strength of the viscous magma plug, fragmentation occurs, resulting in the explosive release of gas and pyroclastic material
326 (e.g. paroxysm). Another possible mechanism, proposed by Suckale et al. (2016) and McKee et al., (2022) suggests that the



327 explosion is triggered by the rapid expansion and release of gas when a partial rupture occurs in the plug at the top of the
328 magma column.

329 **5 Conclusion**

330 The eruptive activity at Stromboli starting from 4, July, and culminating on 11, July 2024, with the paroxysm, provides a
331 comprehensive case study of explosive volcanism at open-conduit volcanoes, thus offering additional insights and proofs for
332 already existing source models.

333 The July 2024 paroxysm is preceded by a prolonged phase of heightened activity, characterized by increased volcanic tremor
334 and VLP events. The high seismicity, combined with observed crater rim collapses and lava flows, suggests a progressive
335 destabilization of the volcanic edifice. In particular, the major explosion on 4, July, and the subsequent paroxysm on 11, July
336 highlight the role of magma gas dynamics, where increased gas volumes and pressure led to significant eruptive events.

337 Seismic analysis reveals that the volcanic tremor intensity is linked to gas-rich magma movement, reaching in this eruptive
338 sequence unprecedented values at Stromboli. However, the variability in VLP events indicates that, while useful for monitoring
339 overall volcano unrest, these signals alone may not serve as reliable precursors for major explosive events. Instead, the
340 combined analysis of different geophysical parameters, including ground deformation, proved crucial for early warning and
341 forecasting as previously suggested by Ripepe et al. (2021a).

342 Ground deformation patterns, specifically the inflation-deflation cycle observed before explosions, align with previous studies,
343 confirming that such patterns reflect the occurrence of imminent explosions regardless of their magnitude. The exponential
344 inflation observed before the paroxysm, caused by gas expansion and the rise of slugs within the magma column, is the same
345 as in other paroxysmal events at Stromboli, supporting the already proposed source mechanism models for explosive events.
346 Through UAS data, Civico et al. (2024) were able to estimate a total volume loss of about 6.0 Mm³ involved after the
347 gravitational mass collapses occurred on 4 and 11 July. The partial collapses generated a reshaping of the summit craters area
348 as well as a deepening 2022 canyon along SdF, thus increasing the flank instability.

349 In conclusion, our results demonstrate how geophysical, visual observation and UAS-derived topographic data could offer
350 valuable insights for tracking the volcanic explosive phenomena as well as the partial collapses of the summit craters due to
351 the flank instability. This multiparametric monitoring approach could lead to significant advancements in reducing volcanic
352 hazards at Stromboli.

353 **Data availability**

354 The seismic waveform data from all the stations are part of INGV seismic network. The data are publicly available at EIDA
355 Italia (<https://eida.ingv.it/>). The infrasound data are available upon request from the INGV- Osservatorio Vesuviano. The
356 infrasonic collected from PISA station are available at <https://doi.org/10.5281/zenodo.14245572>.



357 **Author contribution**

358 L.Z., S.D.A. and P.S. wrote the proposals that funded installation and maintenance of the infrasound array and UAS, designed
359 the field experiment, and financially supported this publication. L.Z. and S.D.A. tested the infrasonic equipment, organized
360 fieldwork and participated in the original design of the experiment. L.Z., S.D.A., R.C., T.R. contributed to assembling the final
361 multiparametric dataset and tested its quality and retrieval. L.Z., R.C. and T.R. installed and maintained the equipment during
362 the field acquisition. M.O. managed and maintained the geophysics network, contributing to the seismo-acoustic data
363 collection. L.Z., S.D.A. and D.G. performed analyses of infrasound data, seismic and tilt data, and prepared all figures. R.C.
364 and T.R. analysed the UAS images. L.Z., D.G. and S.D.A. jointly wrote the initial draft of the manuscript and all authors
365 contributed to review and edit the final version.

366 **Competing interests**

367 The authors declare that they have no conflict of interest.

368 **Acknowledgements**

369 INGV Project ‘Pianeta Dinamico (Dynamic Planet) - Working Earth’: Geosciences For The Understanding The Dynamics Of
370 The Earth And The Consequent Natural Risks - “Dynamo - DYNAMics of eruptive phenoMena at basaltic vOlcanoes”
371 (<https://progetti.ingv.it/it/pian-din/dynamo#project-info>).

372 INGV Departmental Strategic Project “UNO - UNderstanding the Ordinary to forecast the extraordinary: An integrated
373 approach for studying and interpreting the explosive activity at Stromboli volcano” (<https://progetti.ingv.it/it/uno-stromboli>).

374 L.Z., D.G., S.D.A., R.C., T. R. and P.G. are supported by the grant “Progetto INGV Pianeta Dinamico” -Sub-project
375 VT_DYNAMO 2023- code CUP D53J19000170001 - funded by Italian Ministry MIUR (“Fondo Finalizzato al rilancio degli
376 investimenti delle amministrazioni centrali dello Stato e allo sviluppo del Paese”, legge 145/2018).

377 We are indebted to all the colleagues who have contributed to the monitoring efforts on Stromboli during July 2024 and the
378 ones involved in the surveillance and network maintenance activities, to Maria Zagari (Italian Civil Aviation Authority -
379 ENAC) for her help in issuing new NOTAMs during the emergency, and to Giuseppe De Rosa, Istituto Nazionale di
380 Oceanografia e di Geofisica Sperimentale (OGS) for providing the photo of the 11, July paroxysm in Fig. 1.

381 The contents of this article represent the authors’ ideas and do not necessarily correspond to the official opinion and policies
382 of the Dipartimento della Protezione Civile - Presidenza del Consiglio dei Ministri.e UAS images. We are grateful to the
383 “Gruppo monitoring dell'Osservatorio Vesuviano” of INGV, Osservatorio Vesuviano (Italy), for their support in the data
384 management.



385 **Financial support**

386 This work was supported by the grant "Progetto INGV Pianeta Dinamico" -Sub-project VT_DYNAMO 2023- code CUP
387 D53J19000170001 - funded by Italian Ministry MIUR ("Fondo Finalizzato al rilancio degli investimenti delle amministrazioni
388 centrali dello Stato e allo sviluppo del Paese", legge 145/2018) and by NGV Departmental Strategic Project "UNO -
389 UNderstanding the Ordinary to forecast the extraordinary: An integrated approach for studying and interpreting the explosive
390 activity at Stromboli volcano".

391 **References**

- 392 Aiuppa, A., Burton, M., Caltabiano, T., Giudice, G., Guerrieri, S., Liuzzo, M., and Salerno, G.: Unusually large magmatic
393 CO₂ gas emissions prior to a basaltic paroxysm, *Geophys. Res. Lett.*, 37, <https://doi.org/10.1029/2010GL044997>, 2010.
- 394 Andronico, D., Del Bello, E., D'Orlando, C., Landi, P., Pardini, F., Scarlato, P., and Valentini, F.: Uncovering the eruptive
395 patterns of the 2019 double paroxysm eruption crisis of Stromboli volcano, *Nat. Commun.*, 12, [https://doi.org/10.1038/s41467-](https://doi.org/10.1038/s41467-021-23349-4)
396 021-23349-4, 2021.
- 397 Bertagnini, A., Métrich, N., Landi, P., and Rosi, M.: Stromboli volcano (Aeolian Archipelago, Italy): An open window on the
398 deep-feeding system of a steady state basaltic volcano, *J. Geophys. Res. Solid Earth*, 108,
399 <https://doi.org/10.1029/2002JB002146>, 2003.
- 400 Bonaccorso, A.: Evidence of a dyke-sheet intrusion at Stromboli Volcano inferred through continuous tilt, *Geophys. Res. Lett.*,
401 25, <https://doi.org/10.1029/98GL00766>, 1998.
- 402 Burton, M., Allard, P., Murè, F., and La Spina, A.: Magmatic gas composition reveals the source depth of slug-driven
403 Strombolian explosive activity, *Science*, 317, <https://doi.org/10.1126/science.1141900>, 2007.
- 404 Calvari, S., Spampinato, L., and Lodato, L.: The 5 April 2003 vulcanian paroxysmal explosion at Stromboli volcano (Italy)
405 from field observations and thermal data, *J. Volcanol. Geotherm. Res.*, 149, <https://doi.org/10.1016/j.jvolgeores.2005.09.008>,
406 2006.
- 407 Calvari, S., Spampinato, L., Bonaccorso, A., Oppenheimer, C., Rivalta, E., and Boschi, E.: Lava effusion—A slow fuse for
408 paroxysms at Stromboli volcano?, *Earth Planet. Sci. Lett.*, <https://doi.org/10.1016/j.epsl.2011.03.005>, 2011.
- 409 Calvari, S., and Nunnari, G.: Statistical insights on the eruptive activity at Stromboli volcano (Italy) recorded from 1879 to
410 2023, *Remote Sensing*, 15, <https://doi.org/10.3390/rs15174298>, 2023.
- 411 Caricchi, L., Montagna, C. P., Aiuppa, A., Lages, J., Tamburello, G., and Papale, P.: CO₂ flushing triggers paroxysmal
412 eruptions at open conduit basaltic volcanoes, *J. Geophys. Res.: Solid Earth*, 129, <https://doi.org/10.1029/2023JB02561>, 2024.
- 413 Chouet, B., Saccorotti, G., Martini, M., Dawson, P., De Luca, G., Milana, G., and Scarpa, R.: Source and path effects in the
414 wave fields of tremor and explosions at Stromboli Volcano, Italy, *J. Geophys. Res.: Solid Earth*, 102,
415 <https://doi.org/10.1029/96JB03395>, 1997.



- 416 Chouet, B., Dawson, P., Ohminato, T., Martini, M., Saccorotti, G., Giudicepietro, F., De Luca, G., Milana, G., and Scarpa, R.:
417 Source mechanisms of explosions at Stromboli Volcano, Italy, determined from moment-tensor inversions of very-long-period
418 data, *J. Geophys. Res.: Solid Earth*, 108, <https://doi.org/10.1029/2002JB001919>, 2003.
- 419 Chouet, B., Dawson, P., and Martini, M.: Shallow-conduit dynamics at Stromboli Volcano, Italy, imaged from waveform
420 inversions, *Geol. Soc. London, Special Publications*, 307, <https://doi.org/10.1144/SP307.5>, 2008.
- 421 Colò, L., Ripepe, M., Baker, D. R., and Polacci, M.: Magma vesiculation and infrasonic activity at Stromboli open conduit
422 volcano, *Earth Planet. Sci. Lett.*, 292, <https://doi.org/10.1016/j.epsl.2010.01.041>, 2010.
- 423 Civico, R., Ricci, T., Scarlato, P., Andronico, D., Cantarero, M., Carr, B. B., De Beni, E., Del Bello, E., Johnson, J. B.,
424 Kueppers, U., Pizzimenti, L., Schmid, M., Strehlow, K., and Taddeucci, J.: Unoccupied Aircraft Systems (UASs) Reveal the
425 Morphological Changes at Stromboli Volcano (Italy) before, between, and after the 3 July and 28 August 2019 Paroxysmal
426 Eruptions, *Remote Sensing*, 13, <https://doi.org/10.3390/rs13010141>, 2021.
- 427 Civico, R., Ricci, T., Cecili, A., and Scarlato, P.: High-resolution topography reveals morphological changes of Stromboli
428 volcano following the July 2024 eruption, *Sci. Data*, 11, 1219, <https://doi.org/10.1038/s41597-024-04098-y>, 2024.
- 429 D’Auria, L., Giudicepietro, F., Martini, M., and Peluso, R.: Seismological insight into the kinematics of the 5 April 2003
430 vulcanian explosion at Stromboli volcano (southern Italy), *Geophys. Res. Lett.*, 33, <https://doi.org/10.1029/2005GL025502>,
431 2006.
- 432 De Angelis, S., and Bodin, P.: Watching the Wind: Seismic Data Contamination at Long Periods due to Atmospheric Pressure-
433 Field-Induced Tilting, *Bull. Seismol. Soc. Am.*, 102, <https://doi.org/10.1785/0120110245>, 2012.
- 434 Del Bello, E., Llewellyn, E. W., Taddeucci, J., Scarlato, P., and Lane, S. J.: An analytical model for gas overpressure in slug-
435 driven explosions: Insights into Strombolian volcanic eruptions, *J. Geophys. Res.: Solid Earth*, 117(B2),
436 <https://doi.org/10.1029/2011JB008747>, 2012.
- 437 Diaz-Moreno, A., Iezzi, A. M., Lamb, O. D., Fee, D., Kim, K., Zuccarello, L., and De Angelis, S.: Volume Flow Rate
438 Estimation for Small Explosions at Mt. Etna, Italy, From Acoustic Waveform Inversion, *Geophys. Res. Lett.*, 46,
439 <https://doi.org/10.1029/2019GL084159>, 2019.
- 440 Di Traglia, F., Berardino, P., Borselli, L., Calabria, P., Calvari, S., Casalbore, D., et al.: Generation of deposit-derived
441 pyroclastic density currents by repeated crater rim failures at Stromboli Volcano (Italy), *Bull. Volcanol.*, 86,
442 <https://doi.org/10.1007/s00445-024-01516-0>, 2024.
- 443 Delle Donne, D., Tamburello, G., Aiuppa, A., Bitetto, M., Lacanna, G., D’Aleo, R., and Ripepe, M.: Exploring the explosive-
444 effusive transition using permanent ultraviolet cameras, *J. Geophys. Res.: Solid Earth*, 122(6), 4377–4394,
445 <https://doi.org/10.1002/2017JB014027>, 2017.
- 446 European Centre for Medium-Range Weather Forecasts (ECMWF), ECMWF Reanalysis v5. Available at:
447 <https://www.ecmwf.int/en/forecasts/dataset/ecmwf-reanalysis-v5>. Access date: 21 July 2024.



- 448 Fee, D., Izbekov, P., Kim, K., Yokoo, A., Lopez, T., Prata, F., Kazahaya, R., Nakamichi, H., and Iguchi, M.: Eruption mass
449 estimation using infrasound waveform inversion and ash and gas measurements: Evaluation at Sakurajima Volcano, Japan,
450 *Earth Planet. Sci. Lett.*, 480, <https://doi.org/10.1016/j.epsl.2017.09.043>, 2017.
- 451 Fee, D., Toney, L., Kim, K., Sanderson, R. W., Iezzi, A. M., Matoza, R. S., De Angelis, S., Jolly, A. D., Lyons, J. J., and
452 Haney, M. M.: Local Explosion Detection and Infrasound Localization by Reverse Time Migration Using 3-D Finite-
453 Difference Wave Propagation, *Front. Earth Sci.*, 9, <https://doi.org/10.3389/feart.2021.640202>, 2021.
- 454 Francalanci, L., Tommasini, S., and Conticelli, S.: The volcanic activity of Stromboli in the 1906–1998 AD period:
455 mineralogical, geochemical and isotope data relevant to the understanding of the plumbing system, *J. Volcanol. Geotherm.*
456 *Res.*, 131, [https://doi.org/10.1016/S0377-0273\(03\)00364-1](https://doi.org/10.1016/S0377-0273(03)00364-1), 2004.
- 457 Francalanci, L., Davies, G. R., Lustenhouwer, W., Tommasini, S., Mason, P. R. D., and Conticelli, S.: Intra-Grain Sr Isotope
458 Evidence for Crystal Recycling and Multiple Magma Reservoirs in the Recent Activity of Stromboli Volcano, Southern Italy,
459 *J. Petrol.*, 46, <https://doi.org/10.1093/petrology/egi062>, 2005.
- 460 Genco, R., and Ripepe, M.: Inflation-deflation cycles revealed by tilt and seismic records at Stromboli volcano, *Geophys. Res.*
461 *Lett.*, 37, <https://doi.org/10.1029/2009GL042925>, 2010.
- 462 Giordano, G., and De Astis, G.: The summer 2019 basaltic Vulcanian eruptions (paroxysms) of Stromboli, *Bull. Volcanol.*,
463 83, <https://doi.org/10.1007/s00445-020-01403-0>, 2020.
- 464 Giudicepietro, F., Calvari, S., De Cesare, W., Di Lieto, B., Di Traglia, F., Esposito, A. M., Orazi, M., Romano, P., Tramelli,
465 A., Nolesini, T., Casagli, N., Calabria, P., and Macedonio, G.: Seismic and thermal precursors of crater collapses and overflows
466 at Stromboli volcano, *Sci. Rep.*, 13, <https://doi.org/10.1038/s41598-023-30198-9>, 2023.
- 467 Giudicepietro, F., López, C., Macedonio, G., Alparone, S., Bianco, F., Calvari, S., ... and Tramelli, A.: Geophysical precursors
468 of the July-August 2019 paroxysmal eruptive phase and their implications for Stromboli volcano (Italy) monitoring, *Sci. Rep.*,
469 10, 10296, <https://doi.org/10.1038/s41598-020-67160-w>, 2020.
- 470 Gheri, D., Zuccarello, L., De Angelis, S., Ricci, T., and Civico, R.: Infrasonic Data from the July 4–11, 2024 Paroxysm of
471 Stromboli Volcano [Data set]. Zenodo. <https://doi.org/10.5281/zenodo.14245572>, 2024.
- 472 Gurioli, L., Harris, A. J. L., Colò, L., Bernard, J., Favalli, M., Ripepe, M., and Andronico, D.: Classification, landing
473 distribution, and associated flight parameters for a bomb field emplaced during a single major explosion at Stromboli, Italy,
474 *Geology*, 41, <https://doi.org/10.1130/G33576.1>, 2013.
- 475 Harris, A., and Ripepe, M.: Temperature and dynamics of degassing at Stromboli, *J. Geophys. Res.: Solid Earth*, 112(B3),
476 <https://doi.org/10.1029/2006JB004393>, 2007.
- 477 INGV Bulletin of 25/06/2024: [https://www.ct.ingv.it/index.php/monitoraggio-e-sorveglianza/prodotti-del-](https://www.ct.ingv.it/index.php/monitoraggio-e-sorveglianza/prodotti-del-monitoraggio/bollettini-settimanali-multidisciplinari/914-bollettino-Settimanale-sul-monitoraggio-vulcanico-geochimico-e-sismico-del-vulcano-Stromboli-del-2024-06-25/file)
478 [monitoraggio/bollettini-settimanali-multidisciplinari/914-bollettino-Settimanale-sul-monitoraggio-vulcanico-geochimico-e-](https://www.ct.ingv.it/index.php/monitoraggio-e-sorveglianza/prodotti-del-monitoraggio/bollettini-settimanali-multidisciplinari/914-bollettino-Settimanale-sul-monitoraggio-vulcanico-geochimico-e-sismico-del-vulcano-Stromboli-del-2024-06-25/file)
479 [sismico-del-vulcano-Stromboli-del-2024-06-25/file](https://www.ct.ingv.it/index.php/monitoraggio-e-sorveglianza/prodotti-del-monitoraggio/bollettini-settimanali-multidisciplinari/914-bollettino-Settimanale-sul-monitoraggio-vulcanico-geochimico-e-sismico-del-vulcano-Stromboli-del-2024-06-25/file), last access: 19 August 2024.



- 480 INGV Bulletin of 02/07/2024: [https://www.ct.ingv.it/index.php/monitoraggio-e-sorveglianza/prodotti-del-](https://www.ct.ingv.it/index.php/monitoraggio-e-sorveglianza/prodotti-del-monitoraggio/bollettini-settimanali-multidisciplinari/915-bollettino-Settimanale-sul-monitoraggio-vulcanico-geochimico-e-sismico-del-vulcano-Stromboli-del-2024-07-02/file)
481 [monitoraggio/bollettini-settimanali-multidisciplinari/915-bollettino-Settimanale-sul-monitoraggio-vulcanico-geochimico-e-](https://www.ct.ingv.it/index.php/monitoraggio-e-sorveglianza/prodotti-del-monitoraggio/bollettini-settimanali-multidisciplinari/915-bollettino-Settimanale-sul-monitoraggio-vulcanico-geochimico-e-sismico-del-vulcano-Stromboli-del-2024-07-02/file)
482 [sismico-del-vulcano-Stromboli-del-2024-07-02/file](https://www.ct.ingv.it/index.php/monitoraggio-e-sorveglianza/prodotti-del-monitoraggio/bollettini-settimanali-multidisciplinari/915-bollettino-Settimanale-sul-monitoraggio-vulcanico-geochimico-e-sismico-del-vulcano-Stromboli-del-2024-07-02/file), last access: 19 August 2024.
- 483 INGV Bulletin of 09/07/2024: [https://www.ct.ingv.it/index.php/monitoraggio-e-sorveglianza/prodotti-del-](https://www.ct.ingv.it/index.php/monitoraggio-e-sorveglianza/prodotti-del-monitoraggio/bollettini-settimanali-multidisciplinari/918-bollettino-Settimanale-sul-monitoraggio-vulcanico-geochimico-e-sismico-del-vulcano-Stromboli-del-2024-07-09/file)
484 [monitoraggio/bollettini-settimanali-multidisciplinari/918-bollettino-Settimanale-sul-monitoraggio-vulcanico-geochimico-e-](https://www.ct.ingv.it/index.php/monitoraggio-e-sorveglianza/prodotti-del-monitoraggio/bollettini-settimanali-multidisciplinari/918-bollettino-Settimanale-sul-monitoraggio-vulcanico-geochimico-e-sismico-del-vulcano-Stromboli-del-2024-07-09/file)
485 [sismico-del-vulcano-Stromboli-del-2024-07-09/file](https://www.ct.ingv.it/index.php/monitoraggio-e-sorveglianza/prodotti-del-monitoraggio/bollettini-settimanali-multidisciplinari/918-bollettino-Settimanale-sul-monitoraggio-vulcanico-geochimico-e-sismico-del-vulcano-Stromboli-del-2024-07-09/file), last access: 19 August 2024.
- 486 INGV Bulletin of 16/07/2024: [https://www.ct.ingv.it/index.php/monitoraggio-e-sorveglianza/prodotti-del-](https://www.ct.ingv.it/index.php/monitoraggio-e-sorveglianza/prodotti-del-monitoraggio/bollettini-settimanali-multidisciplinari/920-bollettino-Settimanale-sul-monitoraggio-vulcanico-geochimico-e-sismico-del-vulcano-Stromboli-del-2024-07-16/file)
487 [monitoraggio/bollettini-settimanali-multidisciplinari/920-bollettino-Settimanale-sul-monitoraggio-vulcanico-geochimico-e-](https://www.ct.ingv.it/index.php/monitoraggio-e-sorveglianza/prodotti-del-monitoraggio/bollettini-settimanali-multidisciplinari/920-bollettino-Settimanale-sul-monitoraggio-vulcanico-geochimico-e-sismico-del-vulcano-Stromboli-del-2024-07-16/file)
488 [sismico-del-vulcano-Stromboli-del-2024-07-16/file](https://www.ct.ingv.it/index.php/monitoraggio-e-sorveglianza/prodotti-del-monitoraggio/bollettini-settimanali-multidisciplinari/920-bollettino-Settimanale-sul-monitoraggio-vulcanico-geochimico-e-sismico-del-vulcano-Stromboli-del-2024-07-16/file), last access: 19 August 2024.
- 489 James, M. R., Lane, S. J., and Chouet, B. A.: Gas slug ascent through changes in conduit diameter: Laboratory insights into a
490 volcano-seismic source process in low-viscosity magmas, *J. Geophys. Res.: Solid Earth*, 111,
491 <https://doi.org/10.1029/2005JB003718>, 2006.
- 492 Kim, K., and Lees, J. M.: Local Volcano Infrasound and Source Localization Investigated by 3D Simulation, *Seismol. Res.*
493 *Lett.*, 85, <https://doi.org/10.1785/0220130135>, 2014.
- 494 Legrand, D., and Perton, M.: What are VLP signals at Stromboli volcano?, *J. Volcanol. Geotherm. Res.*, 421,
495 <https://doi.org/10.1016/j.jvolgeores.2021.107429>, 2022.
- 496 Longo, R., Lacanna, G., Innocenti, L., and Ripepe, M.: Artificial Intelligence and Machine Learning Tools for Improving Early
497 Warning Systems of Volcanic Eruptions: The Case of Stromboli, *IEEE Trans. Pattern Anal. Mach. Intell.*, 46(12), 7973–7982,
498 <https://doi.org/10.1109/TPAMI.2024.3399689>, 2024.
- 499 Marchetti, E., and Ripepe, M.: Stability of the seismic source during effusive and explosive activity at Stromboli Volcano,
500 *Geophys. Res. Lett.*, 32, <https://doi.org/10.1029/2005GL023962>, 2005.
- 501 Marchetti, E., Genco, R., and Ripepe, M.: Ground deformation and seismicity related to the propagation and drainage of the
502 dyke feeding system during the 2007 effusive eruption at Stromboli volcano (Italy), *J. Volcanol. Geotherm. Res.*, 182,
503 <https://doi.org/10.1016/j.jvolgeores.2009.01.029>, 2009.
- 504 McKee, K. F., Roman, D. C., Waite, G. P., and Fee, D.: Silent very long period seismic events (VLPs) at Stromboli Volcano,
505 Italy, *Geophys. Res. Lett.*, 49(23), e2022GL100735, <https://doi.org/10.1029/2022GL100735>, 2022.
- 506 McNutt, S. R., and Nishimura, T.: Volcanic tremor during eruptions: Temporal characteristics, scaling and constraints on
507 conduit size and processes, *J. Volcanol. Geotherm. Res.*, 178, <https://doi.org/10.1016/j.jvolgeores.2008.07.023>, 2008.
- 508 Pino, N. A., Moretti, R., Allard, P., and Boschi, E.: Seismic precursors of a basaltic paroxysmal explosion track deep gas
509 accumulation and slug upraise, *J. Geophys. Res.: Solid Earth*, 116, <https://doi.org/10.1029/2011JB008547>, 2011.
- 510 Pistolesi, M., Delle Donne, D., Pioli, L., Rosi, M., and Ripepe, M.: The 15 March 2007 explosive crisis at Stromboli volcano,
511 Italy: Assessing physical parameters through a multidisciplinary approach, *J. Geophys. Res.*, 116,
512 <https://doi.org/10.1029/2011JB008527>, 2011.



- 513 Ripepe, M.: Evidence for gas influence on volcanic seismic signals recorded at Stromboli, *J. Volcanol. Geotherm. Res.*, 70,
514 [https://doi.org/10.1016/0377-0273\(96\)00033-8](https://doi.org/10.1016/0377-0273(96)00033-8), 1996a.
- 515 Ripepe, M., Poggi, P., Braun, T., and Gordeev, E.: Infrasonic waves and volcanic tremor at Stromboli, *Geophys. Res. Lett.*,
516 23, <https://doi.org/10.1029/96GL02394>, 1996b.
- 517 Ripepe, M., and Gordeev, E.: Gas bubble dynamics model for shallow volcanic tremor at Stromboli, *J. Geophys. Res.: Solid*
518 *Earth*, 104, <https://doi.org/10.1029/1998JB900046>, 1999.
- 519 Ripepe, M., Delle Donne, D., Lacanna, G., Marchetti, E., and Olivieri, G.: The onset of the 2007 Stromboli effusive eruption
520 recorded by an integrated geophysical network, *J. Volcanol. Geotherm. Res.*, 182(3-4), 131–136,
521 <https://doi.org/10.1016/j.jvolgeores.2009.02.011>, 2009.
- 522 Ripepe, M., Delle Donne, D., Genco, R., Maggio, G., Pistolesi, M., Marchetti, E., Lacanna, G., Olivieri, G., and Poggi, P.:
523 Volcano seismicity and ground deformation unveil the gravity-driven magma discharge dynamics of a volcanic eruption, *Nat.*
524 *Commun.*, 6(1), 6998, <https://doi.org/10.1038/ncomms7998>, 2015.
- 525 Ripepe, M., Pistolesi, M., Coppola, D., Delle Donne, D., Genco, R., Lacanna, G., ... and Valade, S.: Forecasting effusive
526 dynamics and decompression rates by magmastatic model at open-vent volcanoes, *Sci. Rep.*, 7,
527 <https://doi.org/10.1038/s41598-017-00748-4>, 2017.
- 528 Ripepe, M., Lacanna, G., Pistolesi, M., Silengo, M. C., Aiuppa, A., Laiolo, M., ... and Delle Donne, D.: Ground deformation
529 reveals the scale-invariant conduit dynamics driving explosive basaltic eruptions, *Nat. Commun.*, 12, 1683,
530 <https://doi.org/10.1038/s41467-021-21862-y>, 2021a.
- 531 Ripepe, M., Delle Donne, D., Legrand, D., Valade, S., and Lacanna, G.: Magma pressure discharge induces very long period
532 seismicity, *Sci. Rep.*, 11, <https://doi.org/10.1038/s41598-021-86061-x>, 2021b.
- 533 Ripepe, M., and Lacanna, G.: Volcano generated tsunamis recorded in the near source, *Nat. Commun.*, 15,
534 <https://doi.org/10.1038/s41467-024-18567-x>, 2024.
- 535 Rizzo, A. L., Federico, C., Inguaggiato, S., Sollami, A., Tantiello, M., Vita, F., ... and Grassa, F.: The 2014 effusive eruption at
536 Stromboli volcano (Italy): Inferences from soil CO₂ flux and ³He/⁴He ratio in thermal waters, *Geophys. Res. Lett.*, 42,
537 <https://doi.org/10.1002/2015GL064152>, 2015.
- 538 Rosi, M., Bertagnini, A., Harris, A. J. L., Pioli, L., Pistolesi, M., and Ripepe, M.: A case history of paroxysmal explosion at
539 Stromboli: Timing and dynamics of the April 5, 2003 event, *Earth Planet. Sci. Lett.*, 243,
540 <https://doi.org/10.1016/j.epsl.2006.01.035>, 2006.
- 541 Rosi, M., Pistolesi, M., Bertagnini, A., Landi, P., Pompilio, M., and Di Roberto, A.: Chapter 14 Stromboli volcano, Aeolian
542 Islands (Italy): present eruptive activity and hazards, *Geol. Soc., London, Mem.*, 37, <https://doi.org/10.1144/M37.14>, 2013.
- 543 Sparks, R. S. J.: Dynamics of magma degassing, *Geol. Soc., London, Spec. Publ.*, 213,
544 <https://doi.org/10.1144/GSL.SP.2003.213.01.07>, 2003.
- 545 Suckale, J., Keller, T., Cashman, K. V., and Persson, P.-O.: Flow-to-fracture transition in a volcanic mush plug may govern
546 normal eruptions at Stromboli, *Geophys. Res. Lett.*, 43, <https://doi.org/10.1002/2016GL068082>, 2016.



- 547 Wang, S.: Finite-difference time-domain approach to underwater acoustic scattering problems, *J. Acoust. Soc. Am.*, 99,
548 <https://doi.org/10.1121/1.414620>, 1996.